Thermo- and Light-Responsive Polymer-Coated Magnetic Nanoparticles as Potential Drug Carriers

Guihua Cui[1,2], Hao Wang[1†], Shengsen Long[1], Tianshuo Zhang[1], Xiaoyu Guo[3], Shuiying Chen[2], Toyoji Kakuchi[4], Qian Duan[2*] and Donghai Zhao[1*]

[1]Science and Technology Division, Jilin Medical University, Jilin, China, [2]Department of Materials Science and Engineering, Changchun University of Science and Technology, Jilin, China, [3]Jilin Vocational College of Industry and Technology, Jilin, China, [4]Division of Biotechnology and Macromolecular Chemistry, Graduate School of Engineering, Hokkaido University, Sapporo, Japan

A series of thermo- and light-responsive copolymers of poly (*N*-isopropylacrylamide) (PNIPAM) and 6-[4-(4-methoxy phenyl azo)-phenoxyl-hexyl methacrylate) (AzoMA) (PNIPAM-b-PAzoMA) were synthesized *via* reversible addition–fragmentation chain transfer (RAFT) radical polymerization. The resulting copolymers had a narrow molecular weight distribution range of 1.06–1.24, in which M_n changed regularly with the monomer concentration. Subsequently, the diblock copolymers were successfully modified on the surface of iron oxide nanoparticles through the interaction between the chemical bonds to prepare Fe_3O_4@(PNIPAM-b-PAzoMA) nanoparticles. The size of fabricated nanoparticles with excellent thermo-sensitivity and photo-sensitivity was controlled at about 40–50 nm. Cell viability assays suggested that the nanoparticles showed no significant cytotoxicity and potential drug delivery in the tumor microenvironment.

Keywords: Poly(N-isopropylacrylamide) (PNIPAM), magnetic nanoparticles, thermo-sensitive, light-sensitive, Poly(6-[4-(4-methoxy phenyl azo)-phenoxyl- hexyl methacrylate]) (PAzoMA)

1 INTRODUCTION

The cancer burden had risen to 19.3 million new cases and 10.0 million cancer deaths in 2020 (IARC, 2020). Cancer is characterized by highly metastatic and recurrent, traditional treatments such as surgery, chemotherapy, and radiation and is difficult to cure completely (Couzin-Frankel, 2013; Gotwals et al., 2017). Therefore, continuous endeavors by the researchers are being made to develop new low-cost and effective solutions for cancer treatments with few side effects, high specificity, and anti-metastasis (Lu et al., 2020; Baggiolini et al., 2021; Eberhardt et al., 2021). Polymeric nanomedicine has become crucial in clinical application with its precise and efficient targeting therapy of tumors (Farokhzad and Langer, 2006; Hawkins et al., 2008; Girase et al., 2019; Chen et al., 2021). A few drug-carrying polymeric nanoparticles (NPs) have been used in preclinical oncology treatment (Tong et al., 2012; Li et al., 2018; He et al., 2019). Stimulus-responsive NP drug delivery systems have attracted extensive attention because of their specificity, selectivity, and efficacy in tumor tissues and biocompatibility for normal cells (Karimi et al., 2016; Jia et al., 2018). The endogenous and exogenous (or external) stimuli could induce drug release from polymer vesicles. External stimulus-responsive factors included pH, magnetism, temperature, ultrasound, and light

(Satarkar and Hilt, 2008; Brazel, 2009; Schroeder et al., 2009; Ge et al., 2012; Huo et al., 2014; Liu et al., 2014; Shanmugam et al., 2014; Olejniczak et al., 2015; Rwei et al., 2015; Alimoradi et al., 2016). Slight changes in the external environment could trigger the release of the polymer vesicles to the drug. The integration of multiple functions and various chemical nature of compounds to improve their functionalities was an innovative approach to obtaining nanoscale drug carriers.

Light-responsive nanocarriers have attracted extensive attention in the field of drug delivery (Olejniczak et al., 2015; Rwei et al., 2015). Using light as a trigger has many beneficial advantages. Light is easy to manipulate and make tiny adjustments. The photo-responsive nano-carrier acts as a biofriendly material, which could achieve accurate control of the location, time, and dose of released species (Sortino, 2012). The first example is azobenzene units, which could be handily transformed between *trans-* and *cis-*configuration to release encapsulated antineoplastic drugs. There are so many distinctions of azobenzene derivatives in physical, chemical, optical, and biological properties which are caused by *E*-to-*Z* isomerization. It is the reason that azobenzene compounds could be utilized to tune the characteristics of host materials. A growing number of studies were using azobenzene derivatives covalently linked to polymers as photoactivated drug delivery systems in NPs formed *via* self-assembly of polymers (Shibaev et al., 2003; Wang et al., 2015; Zhang et al., 2019; Shi et al., 2021a; Yao et al., 2021). It was reasonable to expect that as soon as the hydrophobic forces and π-π interactions are removed under UV irradiation, the vesicles with drugs dominated by electrostatic forces would expand rapidly to open the "gate" to achieve drug release (Yao et al., 2021).

Fe_3O_4 NPs are excellent nanoparticles for cancer therapy, which have been approved by the U.S. Food and Drug Administration (FDA) for the clinical treatment due to magnetic targeting and T_2-weighted magnetic resonance imaging (MRI) (Ge et al., 2018). However, individual Fe_3O_4 NPs have no antitumor effect. Thus, composite materials based on ions have emerged, especially anti-tumor composites. In recent years, many substances have been used to combine with Fe_3O_4 to prepare antitumor nanoparticles, such as oxide-graphene (Lin et al., 2014), poly (ethylene glycol)-block-poly (lactic-co-glycolic acid) copolymer-encapsulated (Liu et al., 2022), and polymers (Swain et al., 2015; Du et al., 2017; Shi et al., 2021b; Ndebele et al., 2021). These composite Fe_3O_4 NPs showed great potential for cancer therapy. In the past few decades, the temperature sensitivity of poly (*N*-isopropylacrylamide) (PNIPAM) has been utilized to successfully synthesize so many drug nanocarriers with temperature responsiveness and high loading capacity. PNIPAM could respond to changes in the microenvironment temperature, which caused changes in the carrier structure and interactions with cells to achieve temperature-sensitive drug delivery and release (Liu et al., 2015; Bathfield et al., 2016; Nguyen et al., 2016). In our previous study, a series of biomaterials containing PNIPAM were also synthesized, and their lower critical solution temperature (LCST) was close to human body temperature (Cui G. et al., 2020; Cui G. H. et al.,

2020). In this work, we took advantage of the thermo- and light-responsive properties of the polymer to synthesize polymer-coated magnetic nanoparticles, which may be used for drug delivery in the tumor microenvironment.

2 MATERIALS AND METHODS

2.1 Materials and Instrumentation

N- isopropylacrylamide (Aldrich, 98%) was recrystallized twice from a hexane/benzene mixture (3/2, v/v). 2,2′-Azobis (2-methylpropionitrile) (AIBN) (J&K chemical, 98%), 1,3,5-trioxane (Sigma-Aldrich, 99%), 1-dodecanethiol (Sigma-Aldrich, ≥98%), tetrabutylammonium bromide (Sigma-Aldrich, 99%), carbon disulfide (Sigma-Aldrich, 99.9%), p-anisidine (Aladdin, 99%), 1,6-dibromohexane (Aladdin, 99%), phenol (Aladdin, 99%), methacrylic acid (J&K chemical, 98%), and MTT (3-[4,5-dimethylthiazol-2-yl]-2,5-diphenyltetrazolium were purchased from Acros. Human breast cancer cell (MCF-7) culture and NCTC clone 929 (L-929) were purchased from the Type Culture Collection of the Chinese Academy of Sciences, Shanghai.

The ^{1}H nuclear magnetic resonance (NMR) spectra of polymers in $CDCl_3$ were obtained on a Varian Unity 400 NMR spectrometer. The molecular weights (M_n) and polydispersity (M_w/M_n) were measured by gel permeation chromatography (GPC) using a Waters 510 pump and a Model 410 differential refractometer at 25°C. The LCSTs of the polymer solutions were determined by turbidimetry, using a Shimadzu-2600 UV-Vis spectrophotometer with a heating rate of 0.1°C·min^{-1}. FTIR spectra were recorded on a Shimadzu IR-8400S spectrometer. The average particle size and size distribution of the nanoparticles were characterized by dynamic light scattering (DLS) with a Malvern470 instrument at a fixed scattering angle of 90°, after being filtered by 0.45-μm Millipore filters. The scanning electron microscopy (SEM) images were obtained with JEOL JSM-6701SF. The morphologies of the nanoparticles were determined by transmission electron microscopy (TEM) with JEOL JEM-2100. Powder X-Ray Diffraction (XRD) was performed by using an X′-Pert PRO Philips X-ray диffractometer using Cu radiation (wavelength λ is 1.514056 A) in the 2θ range of 10 ~100° with a scan rate of 20°/min. X-ray photoelectron spectra (XPS) were examined on a PHI-5702 instrument using Mg Ka radiation with a pass energy of 29.35 eV. The optical density (OD) was measured at 570 nm with a microplate reader, model 550 (Bio-Rad, United States). Cell viability was determined as a percentage of the negative control (untreated cells).

2.2 General Procedure for the Thermo- and Light-Responsive Block Polymer Synthesis
2.2.1 Synthesis of Dual-responsive Block Polymers
The procedure of AzoMA synthesis is shown in **Supplementary Scheme S1**. $NaNO_2$ (3.0094 g, 43.6 mmol) was dissolved in deionized water (20 ml). Then, it was added to the hydrochloric acid solution of p-anisidine (5.0984 g and 41.4 mmol) solution and stirred at 0°C for 2 h. Miscible liquids were shifted to sodium hydroxide solution (4 g and 0.1 mol) of phenol (4.0902 g and 43.4 mmol) and stirred at 0°C for 2 h, and the pH was adjusted to neutral to obtain 4-hydroxy-4′-

SCHEME 1 | Fabrication strategy for thermo- and light-responsive polymer-coated magnetic nanoparticles.
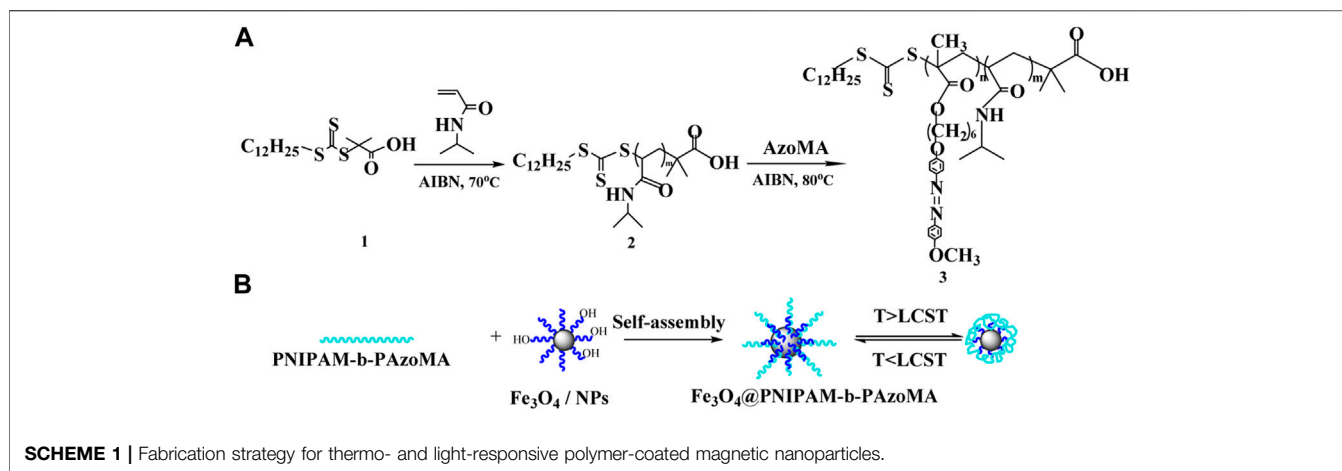
methoxy-azobenzene. The aforementioned product (2.43 g and 10 mmol) and 1, 6-dibromohexane (14.67 g and 53.6 mmol) and anhydrous K_2CO_3 (7.3922 g and 53.6 mmol) were added to acetone (100 ml) and stirred at 75°C for 24 h. The mixture was precipitated in petroleum ether (30~60°C) and recrystallized by thermal filtration in ethyl acetate twice to obtain 1-bromo-6 -(4-methoxyazobenzene-4′-oxygen) hexane.

Methacrylic acid (0.2004 g, 2 mmol) and $KHCO_3$(0.1002 g and 1 mmol) were dissolved in N,N-dimethylformamide(10 ml); then, 1-bromo-6-(4-methoxyazobenzene-4′-oxygen)   hexane(0.3912 g, 1.09 mmol) was added dropwise under whisk and stirred at 65°C for 4 h. The pure AzoMA was acquired by column chromatography (the results are shown in **Supplementary Figures S1, S2**).

2.2.2 Synthesis of PNIPAM-b-PAzoMA
PNIPAM-b-PAzoMA was synthesized using NIPAM and AzoMA as monomers by RAFT, as shown in **Scheme 1**. There were three steps for the synthesis of block copolymers. First, S-1-dodecyl-S'-(α,α'-dimethyl-α''-acetic acid) trithio-carbonate (DMP) (1) was synthesized as a chain transfer agent (CTA). DMP was synthesized by a method derived from Lai et al. (2002), and we have reported in previous research (Cui G. et al., 2020). Subsequently, the synthesis of macromolecular chain transfer agents 2) *via* reversible addition–fragmentation chain transfer (RAFT) was mentioned in our study (Cui G. et al., 2020).

Finally, for the synthesis of PNIPAM-b-PAzoMA, a mixture of AzoMA (0.132 g and 0.5 mmol), macro CTA (152.7 mg and 0.015 mmol), 1,3,5-trioxane (50.44 mg and 0.56 mmol), and AIBN (1.70 mg and 0.01 mmol) was added to anhydrous DMF: H_2O (7.5 ml and 95:5, v/v) and was sealed on the middle side of an H-shaped ampoule glass and stirred. Nitrogen was bubbled through both mixtures for 20 min to remove any oxygen. Three freeze-pump-thaw cycles were performed to degas the solutions. The ampoule was placed at 80°C for 24 h. Polymerization was quenched by exposing the solution to air. The solution was concentrated under a vacuum, and the polymer was precipitated into petroleum ether (30~60°C) thrice; then, the product was dried under a vacuum.

2.3 Synthesis of Polymer-Coated Magnetic Nanoparticles
Fe_3O_4 nanoparticles were synthesized by chemical coprecipitation (Wu et al., 2012). The details are mentioned in our report (Cui G. H. et al., 2020). The Fe_3O_4 nanoparticles were dissolved in N, N-dimethylformamide (20 ml) and dispersed by ultrasonic concussion. Then PNIPAM-b-PAzoMA (0.3 mmol), EDC·HCl (10 mg and 0.052 mmol), and DMAP (7.1 mg and 0.058 mmol) were added successively under stirring and stirred at 80°C in an oil bath for 24 h. The compound was washed continuously with excess methanol in order to remove the unreacted polymer after magnetic separation and dried under vacuum to obtain polymer-coated magnetic nanoparticles.

2.4 Biocompatibility Study
The cell viabilities of macro-CTA, PNIPAM-b-PAzoMA, and Fe_3O_4@PNIPAM-b-PAzoMA nanoparticles were preliminarily investigated by using NCTC clone 929 (L-929) and human breast cancer cell (MCF-7) culture. Specific details were referred to in our previous studies (Cui G. H. et al., 2020). Six replicate wells were used for the control and test concentrations for each sample. The optical density was measured using a microplate reader at 492 nm. The cell viability (%) was calculated according to the following **Eq. 1**:

$$\text{Cell viability}\,(\%) = \left(A_{\text{sample}}/A_{\text{control}}\right) \times 100\%, \qquad (1)$$

where A_{sample} was the absorbance of the cells incubated in DMEM and mixture, and A_{control} was the absorbance of the cells incubated in DMEM.

3 RESULTS AND DISCUSSION

3.1 Architecture Analysis
The morphologies of Fe_3O_4@PNIPAM-b-PAzoMA nanoparticles were investigated by SEM (**Figure 1A**) and TEM (**Figure 1B**). The diameter of the Fe_3O_4@PNIPAM-b-PAzoMA
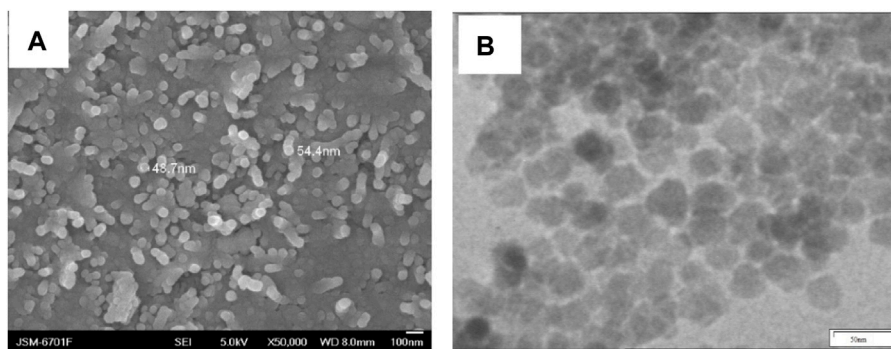
FIGURE 1 | SEM and TEM images of Fe_3O_4@ PNIPAM-b-PAzoMA nanoparticles.
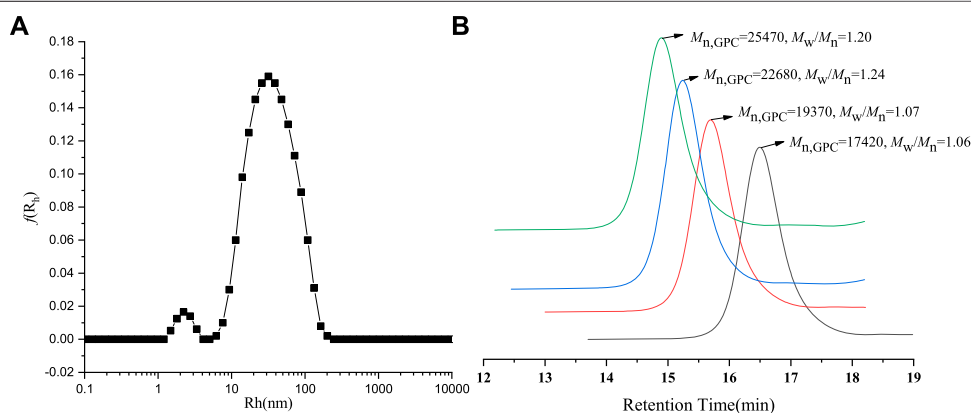
FIGURE 2 | (A) DLS spectrogram for Fe_3O_4@ PNIPAM-b-PAzoMA nanoparticles. **(B)** GPC traces of PNIPAM-b-PAzoMA.
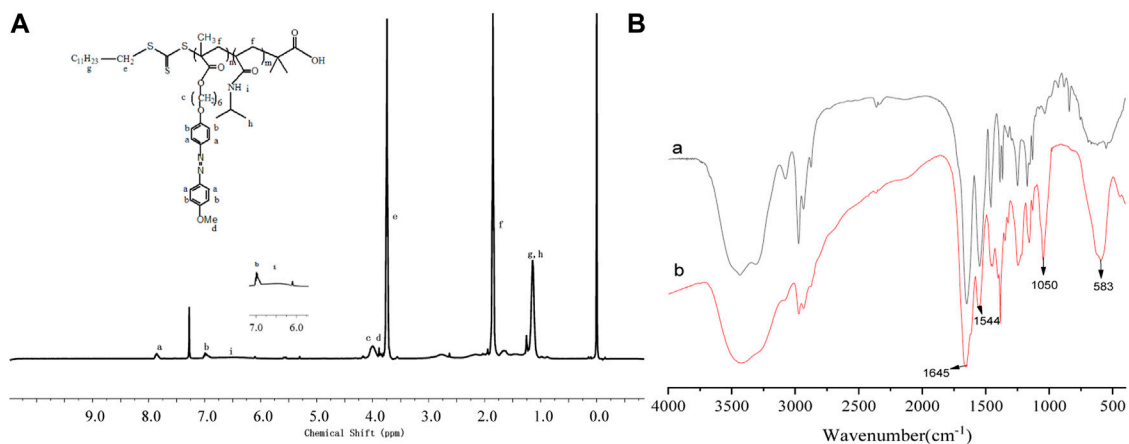
FIGURE 3 | ^{1}HNMR spectra of PNIPAM-b-PAzoMA **(A)**, FT-IR spectra of PNIPAM-b-PAzoMA, and Fe_3O_4@PNIPAM-b-PAzoMA nanoparticles **(B)**.

nanoparticles ranged from 40 to 50 nm. The size was basically identical to the intensity-average hydrodynamic radius distribution f (R_h) which was measured by DLS in **Figure 2A**. The nanoparticles had an almost spherical shape since the

polymer shells of Fe_3O_4@PNIPAM-b-PAzoMA nanoparticles were mostly formed by esterification.

The PNIPAM-b-PAzoMA was synthesized by the different feed ratios of AzoMA/macro-CTA/AIBN, which could obtain
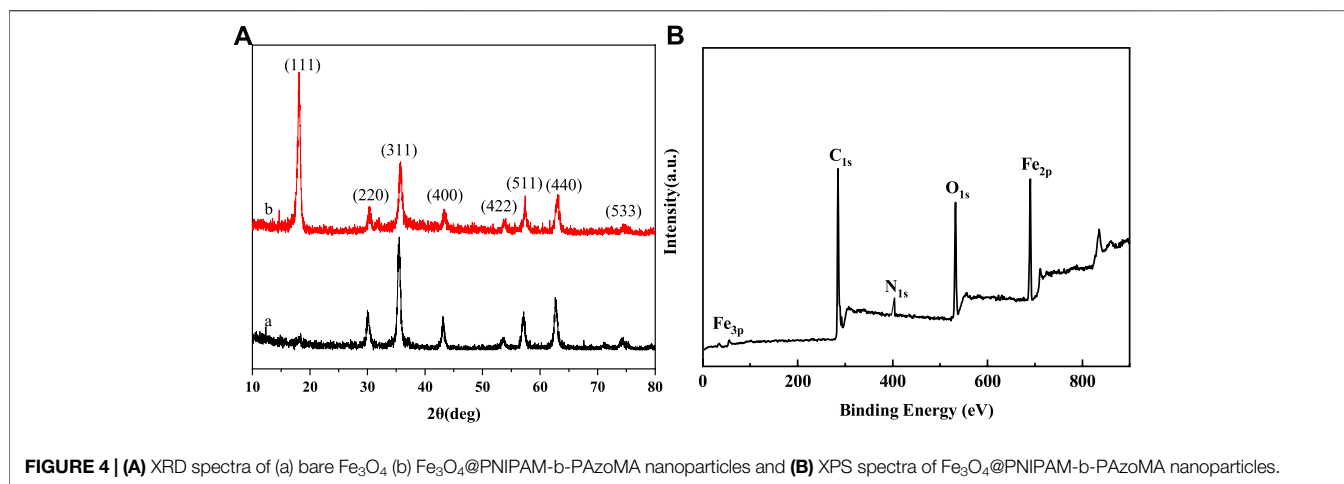
FIGURE 4 | (A) XRD spectra of (a) bare Fe_3O_4 (b) Fe_3O_4@PNIPAM-b-PAzoMA nanoparticles and **(B)** XPS spectra of Fe_3O_4@PNIPAM-b-PAzoMA nanoparticles.
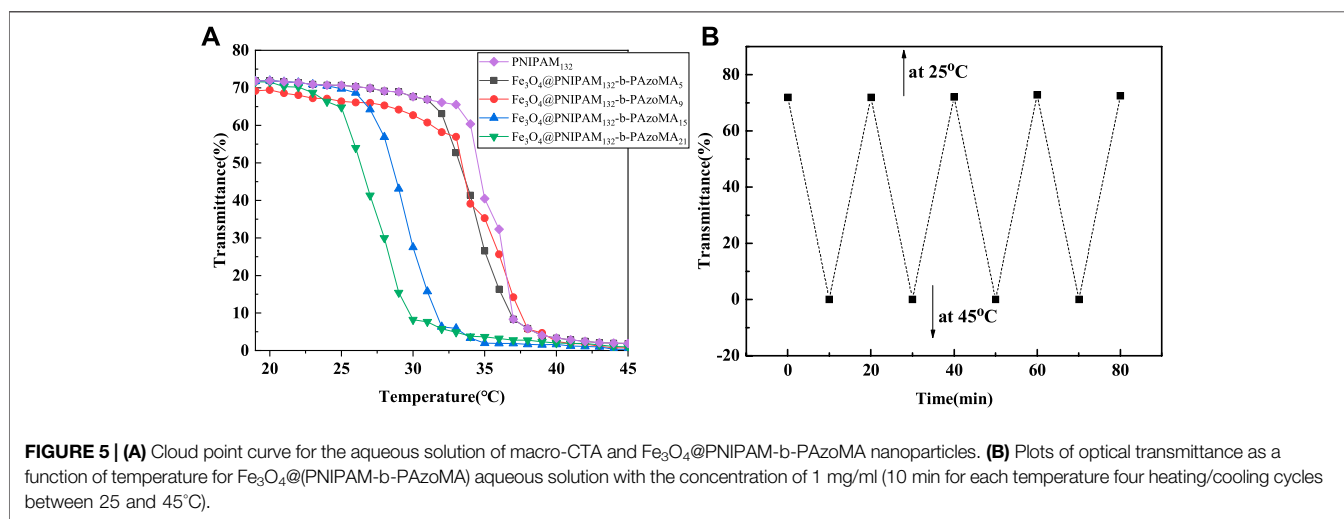
FIGURE 5 | (A) Cloud point curve for the aqueous solution of macro-CTA and Fe_3O_4@PNIPAM-b-PAzoMA nanoparticles. **(B)** Plots of optical transmittance as a function of temperature for Fe_3O_4@(PNIPAM-b-PAzoMA) aqueous solution with the concentration of 1 mg/ml (10 min for each temperature four heating/cooling cycles between 25 and 45°C).

products that had a narrow molecular weight distribution range of 1.06–1.20, as shown in **Figure 2B** and **Supplementary Table S2**. The GPC traces of the block copolymer demonstrated a clean shift toward a lower elution volume. The macro-CTA was a polymer containing 132 PNIPAM units because it had the highest LCST among many macromolecular chain initiators prepared by our study.

The architecture of the PNIPAM-b-PAzoMA and Fe_3O_4@ PNIPAM-b-PAzoMA nanoparticles was authenticated by FT-IR spectra and ¹HNMR. From **Figure 3A**, compared with AzoMA (**Supplementary Figure S1**), a characteristic signal of PNIPAM representing nitrogen atoms was shifted to 6.53 ppm. The peaks at 7.85, 6.98, 3.99, and 3.89 ppm were the characteristic signals of AzoMA. It was seen clearly that the new characteristic peak of PNIPAM at 3,286 cm^{-1} was assigned to the stretching vibration ($\nu_{N–H}$) of the acylamino group in **Figure 3B**. The band at 1,645 $fcm^{-1}$was ascribed to amide I [mainly the carbonyl stretching vibration ($\nu_{C=O}$)], and the band at 1,544cm^{-1} was ascribed to amide II [mainly the N–H bending vibration ($\delta_{N–H}$)], which has overridden the characteristic absorption peaks of AzoMA

because of its high content of PNIPAM in the polymer. Two characteristic peaks appeared in the Fe_3O_4@PNIPAM-b-PAzoMA nanoparticles, which were located in 1,080 cm^{-1} and 583cm^{-1}, and possessed the ester acid bond and Fe-O band.

XPS and XRD spectra were used to further investigate the composition of the nanoparticles. **Figure 4A** showed the XRD pattern of the bare Fe_3O_4 and Fe_3O_4@PNIPAM-b-PAzoMA nanoparticles. The characteristic diffraction peaks for Fe_3O_4 (2θ = 18.07, 30.32, 35.68, 43.32, 53.78, 57.38, 62.89, and 74.56) marked by their indices on (111), (220), (311), (400), (422), (511), (440), and (533) crystal planes can be observed. All the peak positions were basically consistent with the standard data of the Fe_3O_4 structure (JCPDS card file No. 85–1,436) (Cullity, 1978). The peak position did no't change, but the peak intensity changed differently. The dispersion of nanoparticles in the solution was different because of the effect of the surface polymer. In **Figure 4B**, peaks at the binding energies (BEs) of 284.39, 403, and 533.23eV were corresponding to C_{1s}, N_{1s}, and O_{1s}, which were from the copolymer. The BE values of about 55.86eV and 688eV were ascribed to Fe_{3p} and Fe_{2p}. These results indicated that

TABLE 1 | Summarized data on Fe3O4@PNIPAM-b-PAzoMA.

Sample	Amount of AzoMA (mol%)	LCST (%) before irradiation (oC)	LCST after irradiation (oC)	Δ (°C)LCST (oC)
F (°C)e3O4@(PNIPAM132-b-PAzoMA5)	3.6	31.5	31.8	0.3
Fe3O4@(PNIPAM132-b-PAzoMA9)	6.4	30	30.9	0.9
Fe3O4@(PNIPAM132-b-PAzoMA15)	10.2	26.9	29.8	2.9
Fe3O4@(PNIPAM132-b-PAzoMA21)	13.7	25	29	4

FIGURE 6 | (A) Spectral changes of Fe_3O_4@PNIPAM-b-PAzoMA in aqueous solution during UV irradiation (365 nm, 8 W) (a) Fe_3O_4@PNIPAM$_{132}$-b-PAzoMA$_5$, (b) Fe_3O_4@PNIPAM$_{132}$-b-PAzoMA$_9$, (c) Fe_3O_4@PNIPAM$_{132}$-b-PAzoMA$_{15}$, and (d)Fe_3O_4@PNIPAM$_{132}$-b-PAzoMA$_{21}$. **(B)** Spectral changes of Fe_3O_4@PNIPAM$_{132}$-b-PAzoMA$_{21}$ under irradiation time: (a) 0 min, (b) 5 min, (c) 10 min, (d) 15 min, and (e) 20 min.
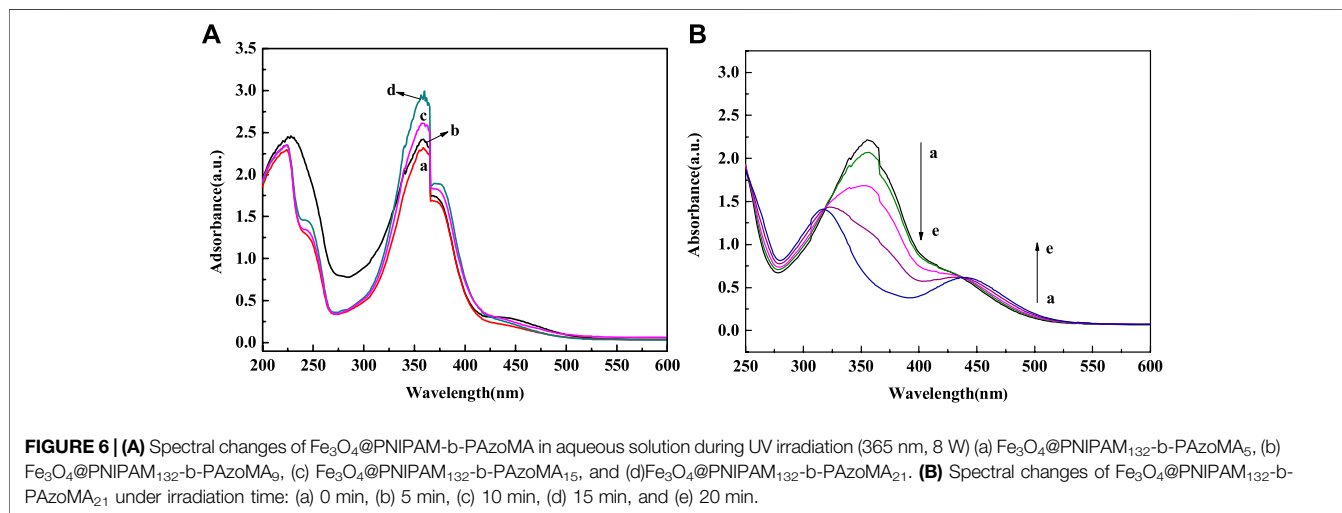
the copolymer was successfully grafted onto the exterior surface of the Fe_3O_4 nanoparticles.

3.2 Thermo- and Light- Responsivity of Nanoparticles

It was found that the LCST of macro-CTA was 33.9°C in **Figure 5A**. It was higher than the homopolymer PNIPAM due to the hydrophilic carboxyl group of the macro-CTA. The LCSTs of all Fe_3O_4@PNIPAM-b-PAzoMA nanoparticles were lower than those of macro-CTA. This might be caused by the hydrophobic interaction of AzoMA in the nanoparticles. Also, the content of AzoMA in nanoparticles was inversely proportional to LCST, as shown in **Supplementary Figure S3**.

The effect of AzoMA's content on the LCST of the polymer was also reflected in the change of LCST of nanoparticles before and after UV irradiation, as shown in **Table 1**. The reason for this phenomenon was that the azo group of AzoMA was in a low dipole moment of the trans configuration without UV irradiation, and the polarity of AzoMA was weak, and this resulted in the strong hydrophobicity of AzoMA, and the LCST of the nanoparticles was lower than that of the macro-CTA. After UV irradiation, the azo group underwent a trans-cis transition. Compared with the trans configuration, the dipole moment of the azo group in the cis configuration was much higher, and the polarity of the AzoMA was also increased so that the hydrophilicity of nanoparticles was significantly enhanced. Another possible reason was that the azo of AzoMA in the trans configuration was a planar configuration.

Compared with the cis structure, the superposition between molecules was more likely to occur so as to enhance the hydrophobic association ability, which was manifested by the increased phase transition temperature of the product after UV irradiation. After the aqueous solution of the sample irradiated by UV light was placed in the shade or exposed to visible light, its LCST returned to the temperature before UV irradiation. This was due to a cis-trans configuration transition of the azo group in **Figure 5B**.

Figure 6 showed the UV spectrum changes of Fe_3O_4@PNIPAM-b-PAzoMA aqueous solutions with different contents of AzoMA that were irradiated by UV light. In the **Figure 6A**, the absorbance was proportional to the content of AzoMA. The sample showed a strong absorption peak at 358 nm, while the absorption peak at 450 nm was relatively weak. This was because AzoMA mainly with its trans configuration under such conditions, and the trans configuration of azobenzene was relatively low. Therefore, this study focused on Fe_3O_4@PNIPAM-b-PAzoMA nanoparticles with high AzoMA contents. However, in **Figure 6B**, the characteristic absorption peak of AzoMA's cis configuration at 450 nm increased with the extension of UV irradiation time. This was because the azo groups in AzoMA gradually changed from trans configuration to cis configuration with the extension of UV irradiation time.

3.3 Thermostability and Magnetism of Nanoparticles

The thermogravimetric analysis (TG) is shown in **Figure 7**. We could clearly determine that below 600°C, after grafting
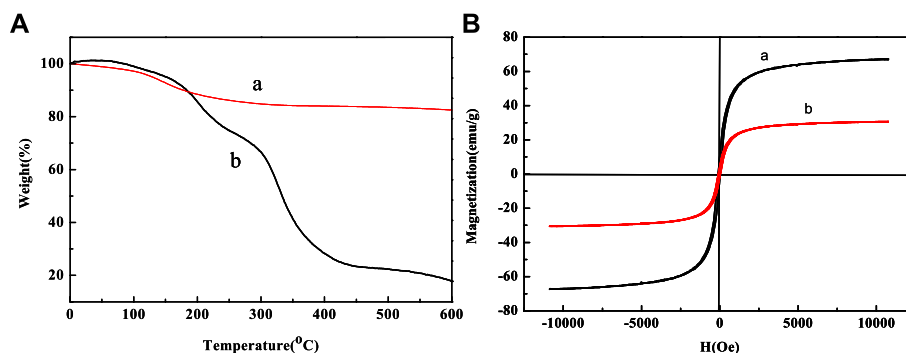
FIGURE 7 | (A) TG curves of (a) Fe_3O_4 and (b) Fe_3O_4@PNIPAM-b-PAzoMA and **(B)** hysteresis loops of (a)bare Fe_3O_4 nanoparticles and (b)Fe_3O_4@PNIPAM-b-PAzoMA nanoparticles at room temperature.
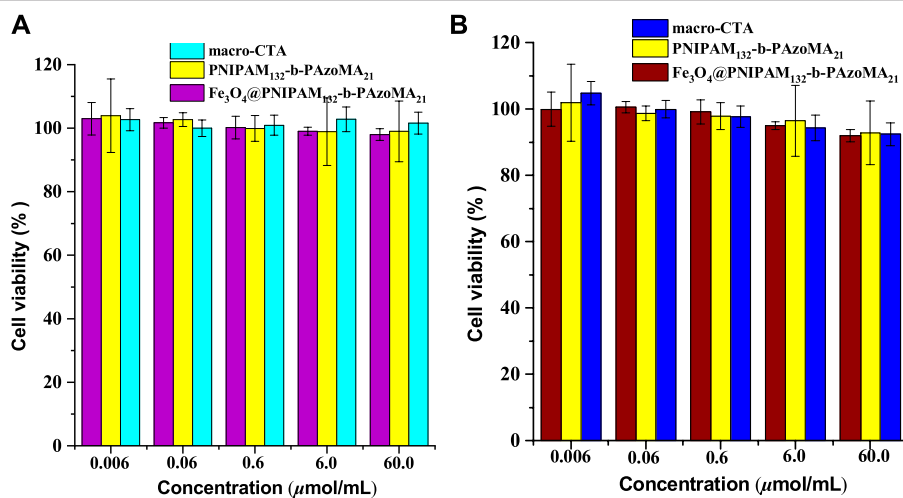
FIGURE 8 | Cell viability of **(A)** the L-929 cells and **(B)** the MCF-7 cells incubated with the samples (macro-CTA, PNIPAM-b-PAzoMA, and Fe_3O_4@PNIPAM-b-PAzoMA nanoparticles), over a range of sample concentrations from 0.006 to 60 μmol/ml by MTT assay for 48 h.

PNIPAM-b-PAzoMA onto the surface of the Fe_3O_4@ PNIPAM-b-PAzoMA nanoparticles, the weight loss was about 56%, while only about 7% of weight loss for bare Fe_3O_4 nanoparticles. Compared with bare Fe_3O_4 nanoparticles, the weight loss of Fe_3O_4@PNIPAM-b-PAzoMA is generally concentrated in three stages which were 70°C~150°C, 150°C~300, and 300°C~500°C. In the first phase, the quality loss was about 5%, which was roughly consistent with the loss in 1), and this value was identified as the loss of Fe_3O_4. The mass loss in the second phase was mainly due to the thermal decomposition of PAzoMA. The weight loss in the third period was relatively large, especially due to the thermal decomposition of PNIPAM in the polymer, which was basically consistent with the data measured by GPC.

Figure 7B shows the hysteresis graph of Fe_3O_4 and Fe_3O_4@ PNIPAM-b-PAzoMA nanoparticles. Due to the small particle size, the saturation magnetization (Ms) of Fe_3O_4 was about 68.02 emu/g. The Ms of Fe_3O_4@PNIPAM-b-PAzoMA

nanoparticles decreased significantly, which was 30.01 emu/g. This was because polymer-coated Fe_3O_4 changed the magnetic anisotropy and increased the directional obstruction on the surface. Fe_3O_4@PNIPAM-b-PAzoMA nanoparticles showed no coercivity, so we could judge that the nanoparticles had a certain degree of super-paramagnetism.

3.4 Assessment of the Cell Viability

The cytotoxicity study on normal cells (L-929, with high activity) and tumor cells (MCF-7, with insensitive to apoptosis induced by various chemotherapeutic drugs) was carried out to investigate the preliminary biocompatibility of the resulting Fe_3O_4@PNIPAM-b-PAzoMA nanoparticles in **Figure 8**. MTT studies showed that macro-CTA, PNIPAM-b-PAzoMA, and Fe_3O_4@PNIPAM-b-PAzoMA nanoparticles had very low toxicity to L-929 cells and MCF-7 cells, and the cell survival rate remained above 80% even at sample concentrations up to 60 μmol/ml.

4 CONCLUSION

In this study, the thermo- and light-responsive polymer-coated magnetic nanoparticles were synthesized. The size of the Fe_3O_4@PNIPAM-b-PAzoMA nanoparticles was about 40–50 nm. Fe_3O_4@PNIPAM-b-PAzoMA nanoparticles had excellent temperature sensitivity, photosensitivity, thermostability, and super-paramagnetism and no significant cytotoxicity. Fe_3O_4@PNIPAM-b-PAzoMA may be used for good drug delivery in the tumor microenvironment and for potential antitumor therapy.

DATA AVAILABILITY STATEMENT

The original contributions presented in the study are included in the article/**Supplementary Material**; further inquiries can be directed to the corresponding authors.

AUTHOR CONTRIBUTIONS

All authors listed have made a substantial, direct, and intellectual contribution to the work and approved it for publication.

SUPPLEMENTARY MATERIAL

The Supplementary Material for this article can be found online at: https://www.frontiersin.org/articles/10.3389/fbioe.2022.931830/full#supplementary-material

REFERENCES

Alimoradi, H., Matikonda, S. S., Gamble, A. B., Giles, G. I., and Greish, K. (2016). Hypoxia Responsive Drug Delivery Systems in Tumor Therapy. *Curr. Pharm. Des.* 22 (19), 2808–2820. doi:10.2174/1381612822666160217130049

Baggiolini, A., Callahan, S. J., Montal, E., Weiss, J. M., Trieu, T., Tagore, M. M., et al. (2021). Developmental Chromatin Programs Determine Oncogenic Competence in Melanoma. *Science* 373, 1–10. doi:10.1126/science.abc1048

Bathfield, M., Reboul, J., Cacciaguerra, T., Lacroix-Desmazes, P., and Gérardin, C. (2016). Thermosensitive and Drug-Loaded Ordered Mesoporous Silica: A Direct and Effective Synthesis Using PEO-B-PNIPAM Block Copolymers. *Chem. Mat.* 28 (10), 3374–3384. doi:10.1021/acs.chemmater.6b00595

Brazel, C. S. (2009). Magnetothermally-responsive Nanomaterials: Combining Magnetic Nanostructures and Thermally-Sensitive Polymers for Triggered Drug Release. *Pharm. Res.* 26 (3), 644–656. doi:10.1007/s11095-008-9773-2

Chen, J., Wang, X., Yuan, Y., Chen, H. T., Zhang, L. P., Xiao, H. H., et al. (2021). Exploiting the Acquired Vulnerability of Cisplatin-Resistant Tumors with a Hypoxia-Amplifying DNA Repair-Inhibiting (HYDRI) Nanomedicine. *Sci. Adv.* 7, 13–25. doi:10.1126/sciadv.abc5267

Couzin-Frankel, J. (2013). Breakthrough of the Year 2013. Cancer Immunotherapy. *Science* 342 (6165), 1432–1433. doi:10.1126/science.342.6165.1432

Cui, G. H., Dong, S. G., Sui, C. H., Duan, Q., and Feng, B. (2020). Fabrication of Composite Fe_3O_4 Nanoparticles Coupled by Thermo-Responsive and Fluorescent Eu Complex on Surface *Int. J. Polym. Mater. Polym. Biomaterials* 8, 1–7.

Cui, G., Zhao, K., You, K., Gao, Z., Kakuchi, T., Feng, B., et al. (2020). Synthesis and Characterization of Phenylboronic Acid-Containing Polymer for Glucose-Triggered Drug Delivery+. *Sci. Technol. Adv. Mater.* 21, 1–10. doi:10.1080/14686996.2019.1700394

Cullity, B. D. (1978). *Elements of X-Ray Diffraction*. Phillippines: Addison-Wesley Publishing Company Inc.

Du, J., Shi, C., Wu, W., Bian, X., Chen, P., Cui, Q., et al. (2017). Synthesis of Core-Shell Structured FAU/SBA-15 Composite Molecular Sieves and Their

Performance in Catalytic Cracking of Polystyrene. *Sci. Technol. Adv. Mater.* 18 (1), 939–949. doi:10.1080/14686996.2017.1396561

Eberhardt, C. S., Kissick, H. T., Patel, M. R., Cardenas, M. A., Prokhnevska, N., Obeng, R. C., et al. (2021). Functional HPV-specific PD-1+ Stem-like CD8 T Cells in Head and Neck Cancer. *Nature* 597, 279–284. doi:10.1038/s41586-021-03862-z

Farokhzad, O., and Langer, R. (2006). Nanomedicine: Developing Smarter Therapeutic and Diagnostic Modalities☆. *Adv. Drug Deliv. Rev.* 58, 1456–1459. doi:10.1016/j.addr.2006.09.011

Ge, J., Neofytou, E., Cahill, T. J., Beygui, R. E., and Zare, R. N. (2012). Drug Release from Electric-Field-Responsive Nanoparticles. *ACS Nano* 6 (1), 227–233. doi:10.1021/nn203430m

Ge, R., Liu, C., Zhang, X., Wang, W., Li, B., Liu, J., et al. (2018). Photothermal-Activatable Fe3O4 Superparticle Nanodrug Carriers with PD-L1 Immune Checkpoint Blockade for Anti-metastatic Cancer Immunotherapy. *ACS Appl. Mat. Interfaces* 10 (24), 20342–20355. doi:10.1021/acsami.8b05876

Girase, M. L., Patil, P. G., and Ige, P. P. (2019). Polymer-drug Conjugates as Nanomedicine: a Review. *Int. J. Polym. Mater. Polym. Biomaterials* 69 (15), 990–1014. doi:10.1080/00914037.2019.1655745

Gotwals, P., Cameron, S., Cipolletta, D., Cremasco, V., Crystal, A., Hewes, B., et al. (2017). Prospects for Combining Targeted and Conventional Cancer Therapy with Immunotherapy. *Nat. Rev. Cancer* 17, 286–301. doi:10.1038/nrc.2017.17

Hawkins, M. J., Soon-Shiong, P., and Desai, N. (2008). Protein Nanoparticles as Drug Carriers in Clinical Medicine. *Adv. Drug Deliv. Rev.* 60, 876–885. doi:10.1016/j.addr.2007.08.044

He, G., Ma, Y., Zhou, H., Sun, S., Wang, X., Qian, H., et al. (2019). Mesoporous NiS2 Nanospheres as a Hydrophobic Anticancer Drug Delivery Vehicle for Synergistic Photothermal-Chemotherapy. *J. Mat. Chem. B* 7, 143–149. doi:10.1039/c8tb02473a

Huo, M., Yuan, J., Tao, L., and Wei, Y. (2014). Redox-responsive Polymers for Drug Delivery: from Molecular Design to Applications. *Polym. Chem.* 5 (5), 1519–1528. doi:10.1039/c3py01192e

IARC (2020). *Latest Global Burden of Cancer Data for 2020*. (Lyon, France: International Agency for Research on Cancer).

Jia, S., Fong, W.-K., Graham, B., and Boyd, B. J. (2018). Photoswitchable Molecules in Long-Wavelength Light-Responsive Drug Delivery: From Molecular Design

to Applications. *Chem. Mat.* 30, 2873–2887. doi:10.1021/acs.chemmater. 8b00357

Karimi, M., Ghasemi, A., Zangabad, P. S., Rahighi, R., Moosavi Basri, S. M., Mirshekari, H., et al. (2016). Smart Micro/nanoparticles in Stimulus-Responsive Drug/gene Delivery Systems. *Chem. Soc. Rev.* 45, 1457–1501. doi:10.1039/c5cs00798d

Lai, J. T., Filla, D., and Shea, R. (2002). Functional Polymers from Novel Carboxyl-Terminated Trithiocarbonates as Highly Efficient RAFT Agents. *Macromolecules* 35, 6754–6756. doi:10.1021/ma020362m

Li, M., Luo, Z., and Zhao, Y. (2018). Self-Assembled Hybrid Nanostructures: Versatile Multifunctional Nanoplatforms for Cancer Diagnosis and Therapy. *Chem. Mat.* 30, 25–53. doi:10.1021/acs.chemmater.7b03924

Lin, L.-S., Cong, Z.-X., Cao, J.-B., Ke, K.-M., Peng, Q.-L., Gao, J., et al. (2014). Multifunctional Fe3O4@Polydopamine Core-Shell Nanocomposites for Intracellular mRNA Detection and Imaging-Guided Photothermal Therapy. *ACS Nano* 8, 3876–3883. doi:10.1021/nn500722y

Liu, F., Kozlovskaya, V., Medipelli, S., Xue, B., Ahmad, F., Saeed, M., et al. (2015). Temperature-Sensitive Polymersomes for Controlled Delivery of Anticancer Drugs. *Chem. Mat.* 27 (23), 7945–7956. doi:10.1021/acs. chemmater.5b03048

Liu, J., Bao, X., Kolesnik, I., Jia, B., Yu, Z., Xing, C., et al. (2022). Enhancing the *In Vivo* Stability of Polycation Gene Carriers by Using PEGylated Hyaluronic Acid as a Shielding System. *BIO Integr* 2 (2), 50–56. doi:10. 15212/bioi-2021-0033

Liu, J., Huang, Y., Kumar, A., Tan, A., Jin, S., Mozhi, A., et al. (2014). pH-Sensitive Nano-Systems for Drug Delivery in Cancer Therapy. *Biotechnol. Adv.* 32 (4), 693–710. doi:10.1016/j.biotechadv.2013.11.009

Lu, S., Wang, Q., Zhang, G., Dong, X., Yang, C. T., Song, Y., et al. (2020). *American Association for Cancer Research (AACR) Annual Meeting 2020.* (New Orleans: LA: American Association for Cancer Research).

Ndebele, R. T., Yao, Q., Shi, Y.-N., Zhai, Y.-Y., Xu, H.-L., Lu, C.-T., et al. (2021). Progress in the Application of Nano- and Micro-based Drug Delivery Systems in Pulmonary Drug Delivery. *BIO Integr.* doi:10. 15212/bioi-2021-0028

Nguyen, M., Felidj, N., and Mangeney, C. (2016). Looking for Synergies in Molecular Plasmonics through Hybrid Thermoresponsive Nanostructures. *Chem. Mat.* 28 (11), 3564–3577. doi:10.1021/acs.chemmater.6b00230

Olejniczak, J., Carling, C.-J., and Almutairi, A. (2015). Photocontrolled Release Using One-Photon Absorption of Visible or NIR Light. *J. Control. Release* 219, 18–30. doi:10.1016/j.jconrel.2015.09.030

Rwei, A. Y., Wang, W., and Kohane, D. S. (2015). Photoresponsive Nanoparticles for Drug Delivery. *Nano Today* 10 (4), 451–467. doi:10.1016/j.nantod.2015. 06.004

Satarkar, N., and Hilt, J. (2008). Magnetic Hydrogel Nanocomposites for Remote Controlled Pulsatile Drug Release. *J. Control. Release* 130 (3), 246–251. doi:10. 1016/j.jconrel.2008.06.008

Schroeder, A., Kost, J., and Barenholz, Y. (2009). Ultrasound, Liposomes, and Drug Delivery: Principles for Using Ultrasound to Control the Release of Drugs from Liposomes. *Chem. Phys. Lipids* 162 (1–2), 1–16. doi:10.1016/j.chemphyslip. 2009.08.003

Shanmugam, V., Selvakumar, S., and Yeh, C.-S. (2014). Near-infrared Light-Responsive Nanomaterials in Cancer Therapeutics. *Chem. Soc. Rev.* 43 (17), 6254–6287. doi:10.1039/c4cs00011k

Shi, C., Wu, Z., Yang, F., and Tang, Y. (2021a). Janus Particles with pH Switchable Properties for High-Efficiency Adsorption of PPCPs in Water. *Solid State Sci.* 119, 106702–106709. doi:10.1016/j.solidstatesciences.2021.106702

Shi, C., Zhang, X., Zhang, X., Chen, P., and Xu, L. (2021b). Ultrasonic Desulfurization of Amphiphilic Magnetic-Janus Nanosheets in Oil-Water Mixture System. *Ultrason. Sonochemistry* 76, 105662–125668. doi:10.1016/j. ultsonch.2021.105662

Shibaev, V., Bobrovsky, A., and Boiko, N. (2003). Photoactive Liquid Crystalline Polymer Systems with Light-Controllable Structure and Optical Properties. *Prog. Polym. Sci.* 28 (5), 729–836. doi:10.1016/s0079-6700(02)00086-2

Sortino, S. (2012). Photoactivated Nanomaterials for Biomedical Release Applications. *J. Mat. Chem.* 22 (2), 301–318. doi:10.1039/c1jm13288a

Swain, A. K., Pradhan, L., and Bahadur, D. (2015). Polymer Stabilized Fe3O4-Graphene as an Amphiphilic Drug Carrier for Thermo-Chemotherapy of Cancer. *ACS Appl. Mat. Interfaces* 7 (15), 8013–8022. doi:10.1021/acsami. 5b02536

Tong, R., Tang, L., and Cheng, J. (2012). Development and Application of Anticancer Nanomedicine. *Cheng J.* 1, 31–46. doi:10.1007/978-1-4614-2305-8_3

Wang, X., Yang, Y., Gao, P., Yang, F., Shen, H., Guo, H., et al. (2015). Synthesis, Self-Assembly, and Photoresponsive Behavior of Tadpole-Shaped Azobenzene Polymers. *ACS Macro Lett.* 4, 1321–1326. doi:10.1021/ acsmacrolett.5b00698

Wu, F., Li, Q., Zhang, X., Liu, L., Wu, S., Sun, D., et al. (2012). Fabrication and Characterization of Thermo-Sensitive Magnetic Polymer Composite Nanoparticles. *J. Magnetism Magnetic Mater.* 324, 1326–1330. doi:10.1016/j. jmmm.2011.11.032

Yao, Y., Yu, Y., Wan, X., Yan, D., Chen, Y., Luo, J., et al. (2021). Azobenzene-Based Cross-Linked Small-Molecule Vesicles for Precise Oxidative Damage Treatments Featuring Controlled and Prompt Molecular Release. *Chem. Mat.* 33, 7357–7366. doi:10.1021/acs.chemmater.1c01860

Zhang, Y., Zhang, Y., Song, G., He, Y., Zhang, X., Liu, Y., et al. (2019). A DNA-Azobenzene Nanopump Fueled by Upconversion Luminescence for Controllable Intracellular Drug Release. *Angew. Chem. Int. Ed.* 58, 18207–18211. doi:10.1002/anie.201909870